ACS APPLIED MATERIALS & INTERFACES

Research Article

www.acsami.org

Design and Synthesis of Target-Responsive Aptamer-Cross-linked Hydrogel for Visual Quantitative Detection of Ochratoxin A

Rudi Liu,[†] Yishun Huang,[†] Yanli Ma,[†] Shasha Jia,[†] Mingxuan Gao,[†] Jiuxing Li,[†] Huimin Zhang,[†] Dunming Xu,[‡] Min Wu,[‡] Yan Chen,[‡] Zhi Zhu,*[,†] and Chaoyong Yang*[,†]

[†]MOE Key Laboratory of Spectrochemical Analysis & Instrumentation, Collaborative Innovation Center of Chemistry for Energy Materials, Key Laboratory for Chemical Biology of Fujian Province, State Key Laboratory of Physical Chemistry of Solid Surfaces, College of Chemistry and Chemical Engineering, Xiamen University Xiamen 361005, China

[‡]Xiamen Entry-Exit Inspection and Quarantine Bureau, Xiamen 361026, China

Supporting Information

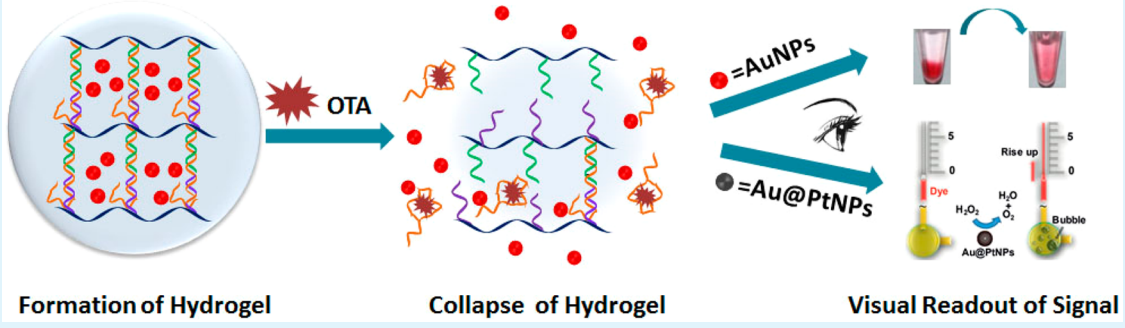

ABSTRACT: A target-responsive aptamer-cross-linked hydrogel was designed and synthesized for portable and visual quantitative detection of the toxin Ochratoxin A (OTA), which occurs in food and beverages. The hydrogel network forms by hybridization between one designed DNA strand containing the OTA aptamer and two complementary DNA strands grafting on linear polyacrylamide chains. Upon the introduction of OTA, the aptamer binds with OTA, leading to the dissociation of the hydrogel, followed by release of the preloaded gold nanoparticles (AuNPs), which can be observed by the naked eye. To enable sensitive visual and quantitative detection, we encapsulated Au@Pt core−shell nanoparticles (Au@PtNPs) in the hydrogel to generate quantitative readout in a volumetric bar-chart chip (V-Chip). In the V-Chip, Au@PtNPs catalyzes the oxidation of H_2O_2 to generate O_2, which induces movement of an ink bar to a concentration-dependent distance for visual quantitative readout. Furthermore, to improve the detection limit in complex real samples, we introduced an immunoaffinity column (IAC) of OTA to enrich OTA from beer. After the enrichment, as low as 1.27 nM (0.51 ppb) OTA can be detected by the V-Chip, which satisfies the test requirement (2.0 ppb) by the European Commission. The integration of a target-responsive hydrogel with portable enrichment by IAC, as well as signal amplification and quantitative readout by a simple microfluidic device, offers a new method for portable detection of food safety hazard toxin OTA.

KEYWORDS: *DNA hydrogel, visual detection, microfluidics, Ochratoxin A*

INTRODUCTION

Ochratoxins, secondary metabolites produced by several species of *Aspergillus* and *Penicillium*,[1,2] are potent toxins that can produce nephrotoxic, teratogenic, carcinogenic, neurotoxic, and immunosuppressive activity.[3−6] There are three members of the Ochratoxin family, A, B, and C, which differ slightly in chemical structure. Ochratoxin A (OTA), the most abundant and toxic subtype,[7−11] has been reported to exist in various food and beverages including cereal, beans, coffee, wine, and beer.[12−15] To date, different countries and organizations have established maximum tolerated levels of OTA in different kinds of food products. The European Commission has set standards for the maximum level of OTA in different food products, including raw cereal grains (5.0 ppb), cereals (3.0 ppb), and beer and grape juice (2.0 ppb).[12,16] Therefore, a sensitive detection method for OTA is needed to meet food safety requirements and prevent the risk of human OTA consumption.

The conventional analytical methods for OTA have been gas chromatography (GC) or high-performance liquid chromatography (HPLC) coupled with UV−vis, fluorescence, or mass spectrometric detectors.[17−23] Despite their accuracy and low detection limit, these methods generally require multiple steps prior to detection, including extraction, preconcentration, and derivatization of the analyte. Moreover, sophisticated equipment with high cost and special technical skills is required.[14] However, significant changes have occurred because the OTA

Received: February 5, 2015
Accepted: March 16, 2015
Published: March 16, 2015

DOI: 10.1021/acsami.5b01120
ACS Appl. Mater. Interfaces 2015, 7, 6982−6990

aptamer was first selected by Cruz-Aguado and Penner in 2008.[24] Because of the easy synthesis, various labeling possibilities, and excellent stability, the OTA aptamer with high binding affinity and good selectivity has appeared as a promising recognition molecule for OTA analysis. A series of assays based on this aptamer have been developed,[25] including fluorescence,[26−28] electrochemical,[29−31] colorimetric transducers,[32,33] piezoelectric ACM,[34] surface-enhanced Raman scattering (SERS),[35,36] and surface plasmon resonance (SPR) immunosensors.[37] Although these methods are sensitive and selective, auxiliary and bulky equipment is still required. To ensure food safety, point-of-care testing for rapid and portable OTA detection without the need for sophisticated instrumentation is highly desirable.

More recently, DNA hydrogels with DNA/DNA or DNA/Aptamer cross-links have been exploited for biosensing, biosepearation, and drug release.[38,39] The hydrogels intelligently swell or collapse upon target recognition, with the advantages of flexibility, stability, cost effectiveness, portability, and ease of storage.[40] Up to now, different kinds of target-responsive DNA hydrogels have been established for portable detection,[41,42] such as small molecules,[40,43,44] ions,[45−48] nucleic acids,[49] and proteins.[50] Previously, we have successfully constructed hydrogels responsive to ATP, cocaine,[43,44] copper ion,[46] and lead ion.[51] Inspired by the exceptional performance of DNA hydrogels as biosensors, target-responsive hydrogel may be an alternative for development of sensitive, specific, user-friendly, rapid, and portable devices for quantitative detection of OTA.

As proof of concept, we chose OTA aptamer as the linker strand (Apt-linker) and two polymer DNA strands A and B (PS-A and PS-B) to form an OTA-responsive DNA hydrogel for portable, rapid, sensitive and visual quantitative detection of OTA. Gold nanoparticles (AuNPs) were first preloaded in the hydrogel as indicator. In the presence of OTA, the cross-links dissociate, releasing AuNPs for colorimetric detection of the concentration of OTA. For further visual quantitative detection, Au@Pt core−shell nanoparticles (Au@PtNPs) with high catalase catalytic efficiency were chosen as another indicator, which could be used in a volumetric bar-chart chip (V-Chip)[52] for quantitative readout. Here OTA was pre-enriched from the real sample using an immunoaffinity column before introducing it to the hydrogel. The movement of the ink bar in the V-Chip pushed by O_2 is proportional to the concentration of target. The proposed method has a detection limit of 1.27 nM (0.51 ppb) OTA in beer, thereby meeting requirements for strict control of OTA content. The results demonstrate that the OTA-responsive hydrogel has the potential to be widely used for rapid, sensitive, and portable detection of OTA in real samples.

EXPERIMENTAL SECTION

Materials and Reagents. The reagents for DNA synthesis were purchased from Glen Research (Sterling, VA, USA). Ammonium persulfate (APS), tetramethylethylenediamine (TEMED), acetate acid and acrylamide were obtained from Sigma-Aldrich (St. Louis, MO, USA). Potassium chloride, sodium chloride, calcium chloride, and tris(hydroxymethyl) aminomethane were purchased from Jinhuada Chemical Reagents (Guangzhou, China). Perfluoro-tri-*n*-butylamine and perfluoro-di-*n*-butylmethylamine were purchased from Minnesota Mining and Manufacturing Company (St.Paul, MN, USA). Other reagents were from Sinopharm Chemical Reagents (Shanghai, China). The immunoaffinity column (IAC) of OTA was supplied by Beijing Thai Le Qi Technology Company (Beijing, China). The OTA reaction buffer contained 10 mM Tris, 120 mM NaCl, 5 mM KCl, and 20 mM $CaCl_2$, (pH 8.5).

Synthesis of Acrylic-DMT Phosphoramidite. Acrylic-DMT phosphoramidite was synthesized to graft DNA strands on polyacrylamide polymer. The synthesis procedure was followed according to our previous report.[53] Briefly, methacrylic acid (176 mg, 2 mmol), 6-amino-2-hydroxymethylhexan-1-ol (294 mg, 2 mmol), N-hydroxybenzotrizole (HOBt, 324 mg, 2.4 mmol), and dicyclohexylcarbodiimide (DCC, 542.4 mg, 2.4 mmol) were dissolved in DMF and stirred at room temperature overnight. Then acrylic-$(OH)_2$ was obtained after purification by column chromatography.

Under dry nitrogen, the acrylic-$(OH)_2$ (270 mg, 1.17 mmol) and 4-dimethylaminopyridine (14 mg, 0.117 mmol) were dissolved in 7 mL of dry pyridine in a 100 mL round-bottom flask in an ice bath, and the dimethoxytrityl chloride (DMT-Cl, 476 mg, 1.404 mmol) was dissolved in 2.5 mL of dry CH_2Cl_2 in a 25 mL round-bottom flask. Then DMT-Cl was added to the former pyridine solution slowly under dry nitrogen in an ice bath with stirring. The reaction flask was removed from the ice bath and allowed to stir at room temperature for 24 h. All solvents were evaporated, and acrylic-DMT was isolated by a column of silica gel using ethyl acetate as the eluent.

Acrylic-DMT (320.7 mg, 0.62 mmol) was dissolved in anhydrous CH_2Cl_2 (1 mL) at 0 °C. Next, N,N′-diisopropylethylamine (DIPEA) (226.2 mg, 1.74 mmol) and 2-cyanoethyldiisopropylchlorophosphoramidite (0.23 mL, 0.74 mmol) were slowly added, and the reaction mixture was allowed to stir at 0 °C for 2 h. After evaporation of the solvents, the residue was dissolved in the mixture of ethyl acetate, petroleum ether, and triethylamine with a ratio of 50:50:3, followed by purification using column chromatography and dehydration to afford the title compound as a colorless oil. The final product was coupled with normal DNA to obtain acrydite-DNA by a DNA synthesizer. ^{1}H NMR (500 MHz, $CDCl_3$) δ 7.41−6.81(m, 13H), 5.63(s, 1H), 5.30(s, 1H), 3.79(s, 6H), 3.72−3.55(m, 6H), 3.25−3.07(m, 4H), 2.54(m, 2H), 1.95(s, 3H), 1.86(m, 1H), 1.49(m, 2H), 1.26(m, 2H), 1.17(d, 6H), 1.12(d, 6H). 31P NMR (202 MHz, CDCl3) δ 147 ppm. ESI-MS Calcd for $C_{41}H_{56}N_3O_6PNa$: 740.87 ($[M + Na]^+$). Found: 741.8.

Synthesis of Oligonucleotides. All oligonucleotides used in this work were synthesized on a 12-column DNA synthesizer (PolyGen GmbH) according to the standard DNA synthesis protocol. DNA strands A and B were modified with acrylic-DMT phosphoramidite at the 3′ and 5′ end, respectively, and the reactions were marked as SA-acr and SB-acr accordingly. After DNA synthesis and modification, the product was cleaved from the solid support, deprotected using saturated ammonia, and purified with an LC3000 semipreparative HPLC system using a reverse-phase C18 column (Chuang Xin Tong Heng, Beijing, China). After detritylation in 80% (v/v) acetate acid, the DNA product was desalted using a NAP-5 column, quantified by UV−vis spectrometer, and stored at −20 °C for future use.

Preparation of Polyacrylamide-DNA Conjugates. SA-acr or SB-acr (500 μM) solution containing 4% acrylamide were pumped by a mechanical pump to remove oxygen at 37 °C for 10 min. Freshly prepared APS (0.15%) and TEMED (0.125%) were introduced to the solution to initiate the polymerization, yielding polyacrylamide-DNA conjugates PS-A and PS-B. A 100k NMWL ultracentrifuge tube was used to remove the residual monomer.

Synthesis and Modification of Nanoparticles. AuNPs with diameters of 13 nm were synthesized following a previously reported method.[54] All glassware used for synthesis was thoroughly washed with freshly prepared aqua regia (HNO_3:HCl = 1:3) and then rinsed with ultrapure water. $HAuCl_4$ solution (100 mL 0.01 wt %) was added to a round-bottom flask and boiled with stirring and refluxing. Then 1 mL 3 wt % sodium citrate was added, and the solution was kept stirring for 30 min. The color of the boiling solution turned red, indicating formation of AuNPs. The solution was allowed to cool to room temperature and stored in the dark before use. UV−vis absorption spectra and TEM were used to characterize the synthesized AuNPs (Figure S1A in the Supporting Information). The concentration of AuNPs was determined to be 2.5 nM by the reported extinction coefficient of 2.46×10^8 $M^{-1}cm^{-1}$.

DOI: 10.1021/acsami.5b01120
ACS Appl. Mater. Interfaces 2015, 7, 6982−6990

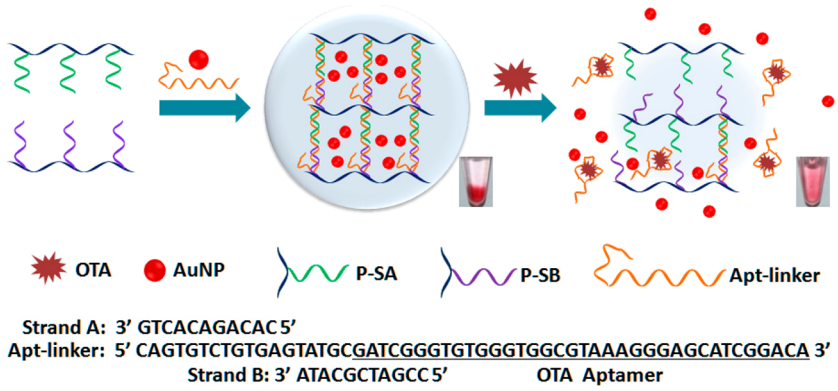

Figure 1. Working principle of the AuNPs encapsulated DNA hydrogel for visual detection of OTA. After introducing OTA, the hydrogel collapses and AuNPs are released, leading to a change of the supernatant from colorless to red, which could be observed by the naked eye.

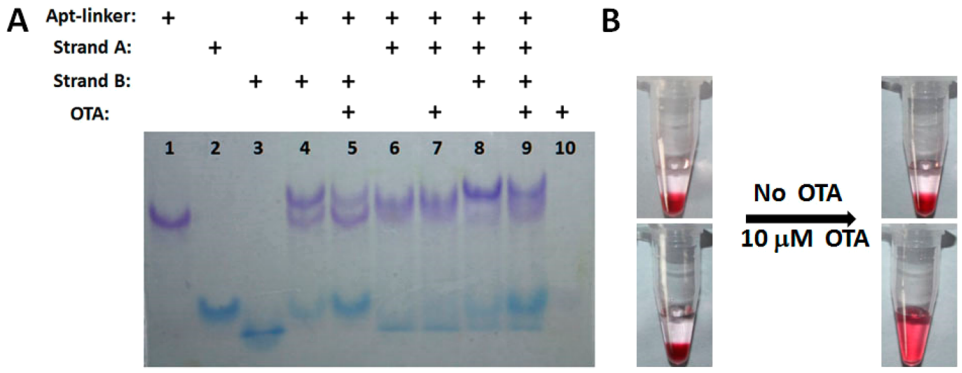

Figure 2. Feasibility of OTA-responsive hydrogel for detection of OTA. (A) Feasibility of disrupting three-strand complex (Strand A—Apt-linker—Strand B) by OTA was confirmed by 15% native PAGE. The concentrations of all DNA were 10 μM and the concentration of OTA was 50 μM. (B) Colorimetric comparison of the response of prepared hydrogel with and without 10 μM OTA.

To synthesize Au@PtNPs, H_2PtCl_6 (200 mL, 3.86 mM) was introduced to 10 mL of the as-synthesized AuNPs and heated to 80 °C with magnetic stirring.[53] Ascorbic acid (400 μL, 10 mM) was slowly dropped into this solution over a 3 min period with a syringe pump, and the mixture was heated and stirred for another 30 min. The diameter of obtained Au@PtNPs was determined by TEM to be around 16 nm.

AuNPs or Au@PtNPs were coated with mPEG-SH (5 kDa) to prevent aggregation in high ionic environments. Briefly, mPEG-SH (50 μL, 20 μM) and Tween20 (0.01 wt %) was added to AuNP or Au@PtNP solution (1 mL, 2.5 nM) and incubated at 37 °C for 30 min. The nanoparticles were then washed three times by centrifugation and resuspension in water, then concentrated to a final concentration of 150 nM.

Design and Fabrication of Volumetric Bar-chart Chip. The V-Chip was designed and fabricated according to our previously reported method.[53] Patterns were drawn using AutoCAD software and sent to Qingyi Precision Maskmaking Co. Ltd. (Shenzhen, China) to generate a film mask. The microchannels on the mask were photolithographically transferred onto the glass surface and etched in a well-stirred etching solution ($HF:HNO_3:H_2O$ = 1:2:17) for 100 min. The holes for inlets and outlets were drilled with a mechanical drill (TBM115, Proxxon). Then the patterned glass was incubated in boiling Piranha solution ($H_2O_2:H_2SO_4$ = 1:3) for 40 min to clean the glass surface. After washing and drying, the surface was fluorinated by dropping 2 wt % 1H, 1H, 2H, 2H-perfluorooctyldimethylchlorosilane/FC40 (a mixture of perfluoro-tri-*n*-butylamine and perfluoro-di-*n*-butylmethylamine) directly onto the surface and baking in an oven at 85 °C for 1 h.

Preparation of OTA-Responsive Hydrogel. To prepare the OTA-responsive DNA hydrogel, we mixed PS-A (2.5 μL, 400 μM), PS-B (2.5 μL, 400 μM), Apt-linker (2.5 μL, 280 μM), and AuNPs (2.5 μL, 30 nM) or Au@PtNPs (2.5 μL, 4.6 nM) and incubated it at 60 °C for 3 min, during which vigorous shaking was used to guarantee homogeneity. The mixture was then slowly cooled to room temperature to generate the hydrogel.

Colorimetric Detection of OTA. Different concentrations of OTA were introduced to 10 μL of hydrogel containing mPEG-SH-protected 13 nm AuNPs. The reaction took place at 25 °C with gentle shaking at 150 rpm for 1.5 h. The color change of the supernatant was recorded by camera to determine the concentration of OTA. Alternatively, UV−vis absorbance of the supernatant was measured for more precise results.

Quantitative Detection of OTA with HV-Chip. Different concentrations of OTA were added to 10 μL of hydrogel containing Au@PtNPs in the reservoir of the HV-Chip and kept at 25 °C for 1.5 h with gentle shaking. The supernatant containing the released Au@PtNPs was drawn to the channel of the HV-Chip by pipet. The upper slide of the chip was raised to mix the Au@PtNPs with H_2O_2 in the channel, leading to generation of O_2, which pushed the ink bar to move. Quantitative detection of the concentration of OTA was obtained by the travel distance of the ink bar.

RESULTS AND DISCUSSION

Working Principle of Target-Responsive Hydrogel for Colorimetric Detection of OTA. The design of OTA-responsive hydrogel is based on our previous studies on target-responsive aptamer-cross-linked hydrogels.[46,51,53] Stoichiometric amounts of DNA strands A and B are grafted onto linear polyacrylamide polymers to form polymer strands A and B (PS-A and PS-B), respectively. As shown in Figure 1, PS-A and PS-B are designed to be complementary to two adjacent areas of the aptamer sequence Apt-linker. When mixed, PS-A and PS-B

DOI: 10.1021/acsami.5b01120
ACS Appl. Mater. Interfaces 2015, 7, 6982−6990

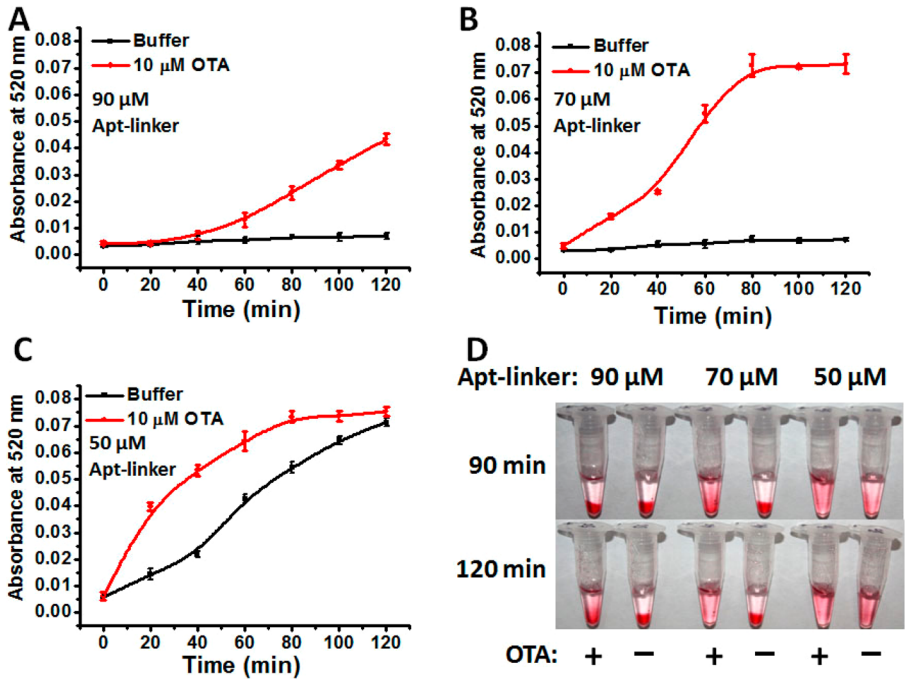

Figure 3. Optimization of the concentrations of Apt-linker to form stable and sensitive target-responsive hydrogel. Kinetics of hydrogel decomposition monitored at 520 nm when (A) 90, (B) 70, and (C) 50 μM Apt-likers were used to cross-link the DNA hydrogel with 100 μM PS-A and PS-B. (D) Images of decomposed DNA hydrogel 90 and 120 min after addition of 0 or 10 μM OTA when different concentrations of Apt-linker were used as linker.

hybridize with Apt-linker through base pairing, thus increasing the cross-linking ratio of the polymer and eventually leading to hydrogel formation. When target OTA molecules are present, OTA aptamer immediately dissociates with strand B and complexes with the toxin molecule, leading to dissolution of the hydrogel and release of the preloaded AuNPs into the supernatant. The change of the supernatant from colorless to red can be observed by the naked eye, and the intensity increases as the concentration of OTA increases.

Feasibility of OTA-Responsive Hydrogel for the Colorimetric Detection of OTA. To validate the cross-linking effect of Apt-linker to DNA strands A and B and the binding ability of Apt-linker to OTA, the hybridization and dehybridization behavior of the three complementary DNA strands were analyzed by native PAGE. As shown in Figure 2A (lanes 1−3), DNA strands A, B, and Apt-liker could be easily distinguished by electrophoresis because of their different lengths. Strand B or A can hybridize with Apt-linker after incubation (lanes 4 and 6). However, the hybridization between strand B and Apt-linker is disturbed by OTA, whereas the hybridization between strand A and Apt-linker is not affected (lanes 5 and 7). This is due to part of the complementary DNA sequence with strand B on Apt-linker belonging to the OTA aptamer, which was an allosteric site and would change its conformation in the presence of OTA. Accordingly, Apt-linker, strand A, and strand B form a three-strand cross-link (lane 8), which dissociates after OTA is introduced (lane 9).

Additional sequences were designed to verify the feasibility. We added a T base on the 5′ of strand A and a C base on 3′ end of strand B, named strand A1 and strand B1, respectively. As shown in Figure S2 in the Supporting Information, the binding efficiency of Apt-linker with OTA was largely reduced when Apt-linker hybridized with strand SB1 instead of strand SB (lanes 5 and 9 in Figure S1 in the Supporting Information, compared with lanes 5 and 9 in Figure 2A). And, compared to SA—Apt-linker—SB, OTA did not efficiently dissociate the three-strand complex (Strand A1—Apt-linker—Strand B1) (lanes 8 and 9 in Figure S1 in the Supporting Information) because the additional T and C bases further enhanced the hybridization strength with Apt-linker. These experiments confirmed that Apt-linker can hybridize with DNA strands A and B efficiently to form a three-strand complex and, equally important, the complex can be efficiently disrupted by the presence of OTA. Hence, DNA strands A and B were chosen to prepare the DNA hydrogel.

To validate the feasibility of the OTA-responsive hydrogel, we chose mPEG-SH-protected 13 nm AuNPs as the indicator embedded in the 3D network. The desalted DNA polymer, PS-A and PS-B, and Apt-linker were incubated at room temperature for 30 min to form the gel after annealing at 60 °C for 3 min with AuNPs. Before introducing OTA, AuNPs on the surface of DNA hydrogel were removed by washing three times with phosphate buffer. As shown in Figure 2B, 10 μM OTA can fully disrupt the hydrogel and rapidly release the AuNPs, leading to the color change of the supernatant solution from colorless to red, whereas AuNPs remained stably loaded in the hydrogel in the absence of OTA.

Optimization of Apt-Linker to Form a Stable and Sensitive OTA-Responsive Hydrogel. To prepare a stable DNA hydrogel with high sensitivity to OTA, we optimized the concentration of Apt-linker. AuNPs were trapped in the target-responsive hydrogel to monitor the hydrogel decomposition. The dissociation kinetics of AuNPs release in the presence of different concentrations of OTA were observed by monitoring the absorbance of AuNPs in the supernatant at 520 nm, which is the absorption maximum for 13 nm AuNPs. As shown in Figure 3A−C, the dissociate rate of hydrogel increased with

DOI: 10.1021/acsami.5b01120
ACS Appl. Mater. Interfaces 2015, 7, 6982−6990

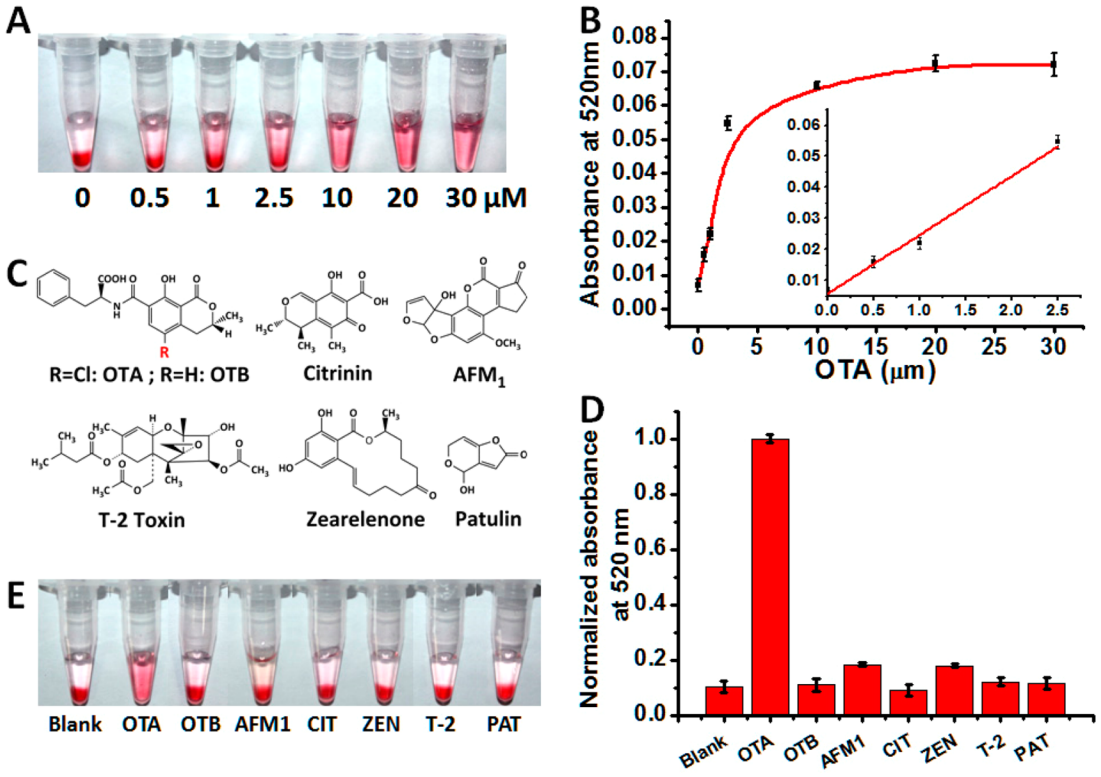

Figure 4. Performance of the AuNP-embedded hydrogel for the detection of OTA. (A) Images showing the decomposition of hydrogel in 120 min when different concentrations of OTA were applied. (B) Standard working curves obtained by monitoring the absorbance of supernatant at 520 nm. (C) Chemical structures of different kinds of toxins, including Ochratoxin B (OTB), Citrinin (CIT), T-2 toxin (T-2), Zearelenone (ZEN), and Patulin (PAT). (D, E) Selective response of DNA hydrogel to 10 μM OTA and other toxins.

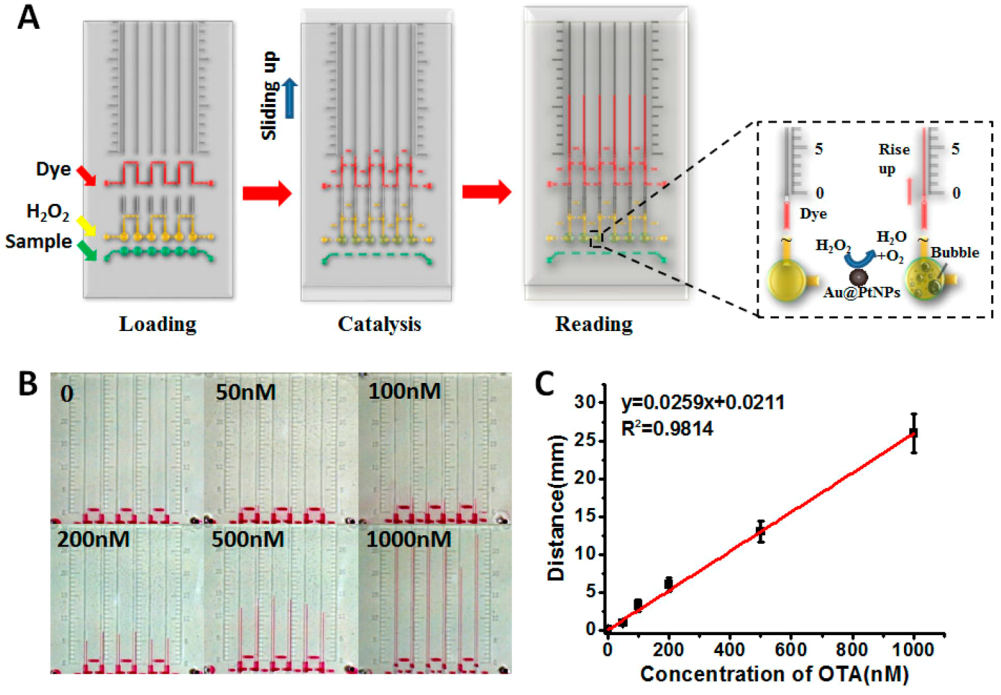

Figure 5. Performance of the HV-Chip for the detection of OTA. (A) Working principle of the target-responsive hydrogel combined with the volumetric bar-chart chip readout for visual quantitative detection. (B) Images showing ink advancement for the detection of OTA in the range of 0 to 1000 nM in 30 min. (C) Linear standard curve was obtained from 0 to 1000 nM OTA.

decreasing concentration of Apt-linker in the presence of 10 μM OTA (red line), indicating increasing sensitivity of the DNA hydrogel to OTA. However, the DNA hydrogel disintegrated even without OTA when 50 μM Apt-linker was used, indicating the weak stability of the DNA hydrogel due to insufficient cross-linkage. Hydrogel images (Figure 3D) also

DOI: 10.1021/acsami.5b01120
ACS Appl. Mater. Interfaces 2015, 7, 6982−6990

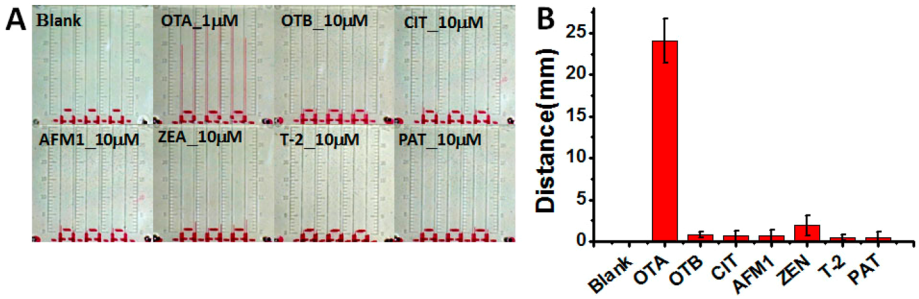

Figure 6. (A) Images showing the selectivity of the HV-Chip method for detection of different kinds of toxins. (B) Travel distance in the HV-Chip in the presence of different kinds of toxins.

obviously show the stability and sensitivity of DNA hydrogel when 70 μM Apt-linker was used. Hence, 70 μM Apt-linker was chosen as the best concentration to prepare stable DNA hydrogels with high sensitivity to OTA.

Sensitive and Selective Detection of OTA with Colorimetric Readout. The performance of the target-responsive hydrogel for colorimetric detection of OTA was evaluated by treating the hydrogel with different concentrations of OTA. As shown in Figure 4A, the supernatant color gradually increased as the target concentration increased. It is reasonable that more Apt-linkers would form OTA-Apt-linker complexes with increasing concentrations of OTA, resulting in increased dissociation of the hydrogel and release of more AuNPs into the supernatant. Figure 4B shows that the absorbance of the supernatant at 520 nm was linearly proportional to the concentration of OTA when the concentration of OTA was below 2.5 μM, establishing the quantitative detection capability of the target-responsive hydrogel. The absorbance gradually reached a plateau when the OTA concentration was above 20 μM, indicating that the hydrogel was completely dissociated. The detection limit was calculated to be 0.24 μM based on the $3\sigma_b$/slope rule.

To demonstrate the specificity of the target-responsive hydrogel for OTA detection, we chose some toxins with similar structures as negative controls. Ten μM samples of each toxin were applied to the hydrogel. As shown in Figure 4D, E, OTA could completely dissociate the DNA hydrogel, whereas other toxins, even with only one atom difference such as OTB, caused little change. The results confirm the ability of target-responsive hydrogel for selective OTA detection.

Portable and Visual Quantitative Detection of OTA with Volumetric Bar-Chart Chip Readout. Colorimetric analysis provides only qualitative or semiquantitative results, which may not satisfy the requirement for precise quantification in certain cases. Moreover, to further decrease the detection limit and increase the sensitivity of target-responsive hydrogel, a volumetric bar-chart chip (V-Chip)[52] was selected as the visual and quantitative readout, as previously integrated with DNA hydrogels for sensitive detection of cocaine[53] and lead ion.[51] The working principle of the target-responsive hydrogel combined with the V-Chip readout (HV-Chip) for visual and quantitative detection is shown in Figure 5A. The V-Chip was fabricated using two glass slides, and six parallel channels with scale marks for single sample testing. The detailed fabrication process could be found in our previous report.[53] Au@PtNPs with excellent catalase catalytic activity were embedded in the hydrogel instead of AuNPs, and different concentrations of OTA were applied. After incubating at room temperature, the supernatant containing released Au@PtNPs was loaded into the channel of V-Chip. At the V-Chip loading position, all horizontal channels are connected, whereas vertical channels are disconnected, keeping Au@PtNPs in the bottom lane, H_2O_2 in the middle lane, and red ink in the top lane. The top layer then moved up to the catalysis position for mixing and reaction, disconnecting the horizontal channels and connecting the vertical channels. Hydrogen peroxide is decomposed by Au@PtNPs to generate O_2, which promotes the advancement of the red ink. The traveling distance of the ink bar can be easily read by the scale mark on the chip. As shown in Figure 5B, the advancements of red ink were proportional to the concentrations of OTA. Figure 5C shows that the distance of red ink movement has a linear relationship with the concentration of OTA. Hence, the hydrogel combined with the V-Chip method can detect OTA concentrations lower than 1 μM in a linear fashion with a detection limit of 10.8 nM, which is about 1 order of magnitude lower than that of the colorimetric readout method. These results clearly demonstrate that the hydrogel integrated with the V-Chip readout can allow quantitative detection of OTA by visually reading the scale with excellent sensitivity.

We further investigated the specificity of HV-Chip method for detection of OTA. Different toxins possessing similar chemical structures (Figure 4C) were applied to OTA aptamer-cross-linked DNA hydrogel. As shown in Figure 6, none of the toxins except OTA could effectively induce advancement of the red ink by generated O_2. Moreover, the concentration of OTA was ten times lower than that of other toxins and there was only one atom difference between OTA and OTB. The results clearly demonstrate the specificity of HV-Chip method for OTA detection.

Determination of OTA in Real Samples. To further investigate the abilities of OTA-responsive HV-Chip system in complex system, we analyzed beer samples spiked with different concentrations of OTA. Beer from a local market was first degassed by ultrasonication and then filtered by 0.22 μm filter membrane to eliminate particulate impurities. The degassed and filtered beer was spiked with different concentrations of OTA and analyzed by the HV-Chip method. As shown in Figure S3 in the Supporting Information, the advancement of red ink was proportional to the concentration of spiked OTA and could detect OTA with a detection limit of 11.1 nM.

For portable detection of trace OTA in the beer, an immunoaffinity column (IAC) packed with antibodies against OTA was introduced to the HV-Chip method (IAC-HV-Chip). IACs of OTA are widely commercialized, as well as easy to obtain and operate, and have the potential to rapidly and conveniently enrich the target toxins from large volume foodstuffs, including the beer. After concentrating OTA from

DOI: 10.1021/acsami.5b01120
ACS Appl. Mater. Interfaces 2015, 7, 6982−6990

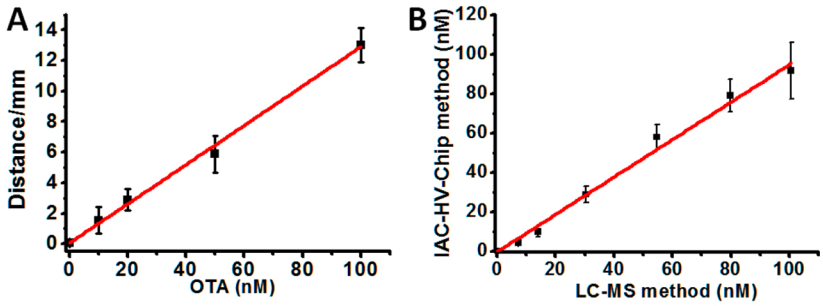

Figure 7. Portable and quantitative detection of OTA by the IAC-HV-Chip method. (A) Standard working curve of IAC-HV-Chip method for the quantification of OTA in the beer from 0 to 100 nM. The detection limit could be obtained as low as 1.27 nM (0.51 ppb). (B) Comparison of the IAC-HV-Chip method with the standard LC-MS method based on 7 beer samples.

the spiked beer by IAC, a portion of the collection was detected by LC-MS/MS for recovery rates (average of 92.5%), and the other portion was analyzed by the HV-Chip method. Figure S4A in the Supporting Information shows the travel distance of the ink bar with different concentrations of OTA in beer after using IACs. From the standard working curve of IAC-HV-Chip method (Figure 7A), the detection limit was further reduced to as low as 1.27 nM (0.51 ppb), which adequately satisfies the test requirements (2.0 ppb) established by the European Commission.

To evaluate the reliability of IAC-HV-Chip method, we also analyzed seven OTA spiked beer samples after enrichment by IAC by LC-MS/MS as the comparison group. The standard working curve of LC-MS/MS method is shown in Figure S4B in the Supporting Information and the contents of OTA in the beer sample were obtained by comparing with the standard working curve after LC-MS/MS analysis. Figure 7B shows a plot of the OTA concentrations determined by IAC-HV-Chip versus equivalent concentrations determined by LC-MS/MS, and a slope of 0.9812 was observed, suggesting that the results analyzed by IAC-HV-Chip method perfectly matched with those of the LC-MS/MS method. The results here clearly demonstrate that the OTA-responsive hydrogel can be widely used for portable, rapid, and highly sensitive detection of OTA in real samples.

CONCLUSIONS

We have successfully designed and synthesized a toxin-responsive DNA hydrogel for the first time, allowing for portable and visual quantitative detection of OTA in real samples. The hydrogel can be loaded with AuNPs for simple and visual colorimetric analysis, particularly useful for detection on site. Furthermore, combining the enrichment of IAC with high catalytic efficiency of Au@PtNPs and portable readout of V-Chip, the IAC-HV-Chip method showed suitability for point-of-care testing of OTA with high sensitivity with a low detection limit of 1.27 nM (0.51 ppb) in beer, enabling trace detection of OTA in real samples. Meanwhile, the hydrogel has high selectivity for OTA, and can effectively distinguish other toxins even with one atom difference, such as OTB. As a variety of aptamers against a broad range of targets can be obtained through SELEX, the IAC-HV-Chip method can also be developed as a powerful tool for the analysis of other toxins. Hence, the IAC-HV-Chip method with the advantages of high sensitivity, selectivity, versatility, robustness, low cost, and portability without electrical power has great potential for quantitative point-of-care testing to ensure food safety and human health.

ASSOCIATED CONTENT

Supporting Information

TEM images of 13 nm AuNPs and 16 nm Au@PtNPs (Figure S1), investigation of feasibility of Strand A1, Strand B1 with Apt-linker by 15% native PAGE (Figure S2), detection of OTA in beer by the HV-Chip method (Figure S3), analysis of OTA in beer by the IAC-HV-Chip method (Figure S4A), standard working curve of LC-MS method for the quantification of OTA (Figure S4B). This material is available free of charge via the Internet at http://pubs.acs.org.

AUTHOR INFORMATION

Corresponding Authors

*Tel: (+86) 592-218-7601. Fax: (+86) 592-218-9959. E-mail: cyyang@xmu.edu.cn.
*E-mail: zhuzhi@xmu.edu.cn.

Author Contributions

The manuscript was written through contributions of all authors. All authors have given approval to the final version of the manuscript.

Notes

The authors declare no competing financial interest.

ACKNOWLEDGMENTS

We thank the National Natural Science Funds for Distinguished Young Scholar (21325522), National Natural Science Funds for Excellent Youth Scholars of China (21422506), the National Natural Science Foundation of China (91313302, 21205100, 21275122, 21435004), National Instrumentation Program (2011YQ03012412), Natural Science Foundation of Fujian Province (2013J01061), and the National Found for Fostering Talents of Basic Science (NFFTBS, J1310024) for their financial support.

REFERENCES

(1) Varga, J.; Kevei, E.; Rinyu, E.; Teren, J.; Kozakiewicz, Z. Ochratoxin Production by Aspergillus Species. *Appl. Environ. Microbiol.* **1996**, *62*, 4461−4464.
(2) Bayman, P.; Baker, J. L.; Doster, M. A.; Michailides, T. J.; Mahoney, N. E. Ochratoxin Production by the Aspergillus Ochraceus Group and Aspergillus Alliaceus. *Appl. Environ. Microbiol.* **2002**, *68*, 2326−2329.
(3) Krogh, P. Role of Ochratoxin in Disease Causation. *Food Chem. Toxicol.* **1992**, *30*, 213−24.
(4) Mantle, P. G. Risk Assessment and the Importance of Ochratoxins. *Int. Biodeterior. Biodegrad.* **2002**, *50*, 143−146.
(5) Walker, R. Risk Assessment of Ochratoxin: Current Views of the European Scientific Committee on Food, the Jecfa, and the Codex

DOI: 10.1021/acsami.5b01120
ACS Appl. Mater. Interfaces 2015, 7, 6982−6990

Committee on Food Additives and Contaminants. *Adv. Exp. Med. Biol.* **2002**, *504*, 249−255.
(6) Reddy, L.; Bhoola, K. Ochratoxins - Food Contaminants: Impact on Human Health. *Toxins* **2010**, *2*, 771−779.
(7) Li, S.; Marquardt, R. R.; Frohlich, A. A.; Vitti, T. G.; Crow, G. Pharmacokinetics of Ochratoxin a and Its Metabolites in Rats. *Toxicol. Appl. Pharmacol.* **1997**, *145*, 82−90.
(8) Manderville, R. A. A Case for the Genotoxicity of Ochratoxin a by Bioactivation and Covalent DNA Adduction. *Chem. Res. Toxicol.* **2005**, *18*, 1091−1097.
(9) Mosesso, P.; Cinelli, S.; Piñero, J.; Bellacima, R.; Pepe, G. In Vitro Cytogenetic Results Supporting a DNA Nonreactive Mechanism for Ochratoxin a, Potentially Relevant for Its Carcinogenicity. *Chem. Res. Toxicol.* **2008**, *21*, 1235−1243.
(10) Pfohl-Leszkowicz, A.; Manderville, R. A. An Update on Direct Genotoxicity as a Molecular Mechanism of Ochratoxin a Carcinogenicity. *Chem. Res. Toxicol.* **2011**, *25*, 252−262.
(11) Klarić, M.; Rašić, D.; Peraica, M. Deleterious Effects of Mycotoxin Combinations Involving Ochratoxin A. *Toxins* **2013**, *5*, 1965−1987.
(12) Covarelli, L.; Beccari, G.; Marini, A.; Tosi, L. A Review on the Occurrence and Control of Ochratoxigenic Fungal Species and Ochratoxin a in Dehydrated Grapes, Non-Fortified Dessert Wines and Dried Vine Fruit in the Mediterranean Area. *Food Control* **2012**, *26*, 347−356.
(13) Wu, X.; Hu, J.; Zhu, B.; Lu, L.; Huang, X.; Pang, D. Aptamer-Targeted Magnetic Nanospheres as a Solid-Phase Extraction Sorbent for Determination of Ochratoxin a in Food Samples. *J. Chromatogr. A* **2011**, *1218*, 7341−7346.
(14) Ahmed, N. E.; Farag, M. M.; Soliman, K. M.; Abdel-Samed, A. K. M.; Naguib, K. M. Evaluation of Methods Used to Determine Ochratoxin a in Coffee Beans. *J. Agric. Food. Chem.* **2007**, *55*, 9576−9580.
(15) Imperato, R.; Campone, L.; Piccinelli, A. L.; Veneziano, A.; Rastrelli, L. Survey of Aflatoxins and Ochratoxin a Contamination in Food Products Imported in Italy. *Food Control* **2011**, *22*, 1905−1910.
(16) Quintela, S.; Villarán, M. C.; López de Armentia, I.; Elejalde, E. Ochratoxin a Removal in Wine: A Review. *Food Control* **2013**, *30*, 439−445.
(17) Castegnaro, M.; Maru, V.; Maru, G.; Ruiz-Lopez, M. D. High-Performance Liquid Chromatographic Determination of Ochratoxin a and Its 4r-4-Hydroxy Metabolite in Human Urine. *Analyst* **1990**, *115*, 129−31.
(18) Studer-Rohr, I.; Dietrich, D. R.; Schlatter, J.; Schlatter, C. The Occurrence of Ochratoxin a in Coffee. *Food Chem. Toxicol.* **1995**, *33*, 341−55.
(19) Soleas, G. J.; Yan, J.; Goldberg, D. M. Assay of Ochratoxin a in Wine and Beer by High-Pressure Liquid Chromatography Photodiode Array and Gas Chromatography Mass Selective Detection. *J. Agric. Food Chem.* **2001**, *49*, 2733−2740.
(20) Becker, M.; Degelmann, P.; Herderich, M.; Schreier, P.; Humpf, H.-U. Column Liquid Chromatography-Electrospray Ionization-Tandem Mass Spectrometry for the Analysis of Ochratoxin. *J. Chromatogr. A* **1998**, *818*, 260−264.
(21) Pittet, A.; Royer, D. Rapid, Low Cost Thin-Layer Chromatographic Screening Method for the Detection of Ochratoxin a in Green Coffee at a Control Level of 10 Mg/kg. *J. Agric. Food Chem.* **2002**, *50*, 243−247.
(22) Losito, I.; Monaci, L.; Palmisano, F.; Tantillo, G. Determination of Ochratoxin a in Meat Products by High-Performance Liquid Chromatography Coupled to Electrospray Ionisation Sequential Mass Spectrometry. *Rapid Commun. Mass Spectrom.* **2004**, *18*, 1965−1971.
(23) Duarte, S. C.; Lino, C. M.; Pena, A. Novel Iac-Lc-Esi-Ms2 Analytical Set-up for Ochratoxin a Determination in Pork. *Food Chem.* **2013**, *138*, 1055−1061.
(24) Cruz-Aguado, J. A.; Penner, G. Determination of Ochratoxin a with a DNA Aptamer. *J. Agric. Food Chem.* **2008**, *56*, 10456−10461.
(25) Hayat, A.; Yang, C.; Rhouati, A.; Marty, J. L. Recent Advances and Achievements in Nanomaterial-Based, and Structure Switchable Aptasensing Platforms for Ochratoxin a Detection. *Sensors* **2013**, *13*, 15187−15208.
(26) Wei, Y.; Zhang, J.; Wang, X.; Duan, Y. Amplified Fluorescent Aptasensor through Catalytic Recycling for Highly Sensitive Detection of Ochratoxin A. *Biosens. Bioelectron.* **2015**, *65*, 16−22.
(27) Chen, J.; Zhang, X.; Cai, S.; Wu, D.; Chen, M.; Wang, S.; Zhang, J. A Fluorescent Aptasensor Based on DNA-Scaffolded Silver-Nanocluster for Ochratoxin a Detection. *Biosens. Bioelectron.* **2014**, *57*, 226−231.
(28) Zhao, Q.; Lv, Q.; Wang, H. Identification of Allosteric Nucleotide Sites of Tetramethylrhodamine-Labeled Aptamer for Noncompetitive Aptamer-Based Fluorescence Anisotropy Detection of a Small Molecule, Ochratoxin A. *Anal. Chem.* **2014**, *86*, 1238−1245.
(29) Jiang, L.; Qian, J.; Yang, X.; Yan, Y.; Liu, Q.; Wang, K.; Wang, K. Amplified Impedimetric Aptasensor Based on Gold Nanoparticles Covalently Bound Graphene Sheet for the Picomolar Detection of Ochratoxin A. *Anal. Chim. Acta* **2014**, *806*, 128−135.
(30) Chen, Y.; Yang, M.; Xiang, Y.; Yuan, R.; Chai, Y. Binding-Induced Autonomous Disassembly of Aptamer-Dnazyme Super-sandwich Nanostructures for Sensitive Electrochemiluminescence Turn-on Detection of Ochratoxin A. *Nanoscale* **2014**, *6*, 1099−1104.
(31) Evtugyn, G.; Porfireva, A.; Stepanova, V.; Kutyreva, M.; Gataulina, A.; Ulakhovich, N.; Evtugyn, V.; Hianik, T. Impedimetric Aptasensor for Ochratoxin a Determination Based on Au Nanoparticles Stabilized with Hyper-Branched Polymer. *Sensors* **2013**, *13*, 16129−16145.
(32) Wang, L.; Ma, W.; Chen, W.; Liu, L.; Ma, W.; Zhu, Y.; Xu, L.; Kuang, H.; Xu, C. An Aptamer-Based Chromatographic Strip Assay for Sensitive Toxin Semi-Quantitative Detection. *Biosens. Bioelectron.* **2011**, *26*, 3059−3062.
(33) Yang, C.; Wang, Y.; Marty, J.-L.; Yang, X. Aptamer-Based Colorimetric Biosensing of Ochratoxin a Using Unmodified Gold Nanoparticles Indicator. *Biosens. Bioelectron.* **2011**, *26*, 2724−2727.
(34) Vidal, J. C.; Duato, P.; Bonel, L.; Castillo, J. R. Use of Polyclonal Antibodies to Ochratoxin a with a Quartz-Crystal Microbalance for Developing Real-Time Mycotoxin Piezoelectric Immunosensors. *Anal. Bioanal. Chem.* **2009**, *394*, 575−582.
(35) Ganbold, E.-O.; Lee, C. M.; Cho, E.-M.; Son, S. J.; Kim, S.; Joo, S.-W.; Yang, S. I. Subnanomolar Detection of Ochratoxin a Using Aptamer-Attached Silver Nanoparticles and Surface-Enhanced Raman Scattering. *Anal. Methods* **2014**, *6*, 3573−3577.
(36) Galarreta, B. C.; Tabatabaei, M.; Guieu, V.; Peyrin, E.; Lagugne-Labarthet, F. Microfluidic Channel with Embedded Sers 2d Platform for the Aptamer Detection of Ochratoxin A. *Anal. Bioanal. Chem.* **2013**, *405*, 1613−1621.
(37) Shankaran, D. R.; Gobi, K. V.; Miura, N. Recent Advancements in Surface Plasmon Resonance Immunosensors for Detection of Small Molecules of Biomedical, Food and Environmental Interest. *Sens. Actuators, B* **2007**, *121*, 158−177.
(38) Battig, M. R.; Soontornworajit, B.; Wang, Y. Programmable Release of Multiple Protein Drugs from Aptamer-Functionalized Hydrogels Via Nucleic Acid Hybridization. *J. Am. Chem. Soc.* **2012**, *134*, 12410−12413.
(39) Wu, Y.; Li, C.; Boldt, F.; Wang, Y.; Kuan, S. L.; Tran, T. T.; Mikhalevich, V.; Foertsch, C.; Barth, H.; Yang, Z.; Liu, D.; Weil, T. Programmable Protein-DNA Hybrid Hydrogels for the Immobilization and Release of Functional Proteins. *Chem. Commun.* **2014**, *50*, 14620−14622.
(40) Yang, H.; Liu, H.; Kang, H.; Tan, W. Engineering Target-Responsive Hydrogels Based on Aptamer - Target Interactions. *J. Am. Chem. Soc.* **2008**, *130*, 6320−6321.
(41) Xiong, X. L.; Wu, C. C.; Zhou, C. S.; Zhu, G. Z.; Chen, Z.; Tan, W. H. Responsive DNA-Based Hydrogels and Their Applications. *Macromol. Rapid Commun.* **2013**, *34*, 1271−1283.
(42) Khimji, I.; Kelly, E. Y.; Helwa, Y.; Hoang, M.; Liu, J. Visual Optical Biosensors Based on DNA-Functionalized Polyacrylamide Hydrogels. *Methods* **2013**, *64*, 292−298.
(43) Yan, L.; Zhu, Z.; Zou, Y.; Huang, Y. S.; Liu, D. W.; Jia, S. S.; Xu, D. M.; Wu, M.; Zhou, Y.; Zhou, S.; Yang, C. J. Target-Responsive

DOI: 10.1021/acsami.5b01120
ACS Appl. Mater. Interfaces 2015, 7, 6982−6990

"Sweet" Hydrogel with Glucometer Readout for Portable and Quantitative Detection of Non-Glucose Targets. *J. Am. Chem. Soc.* **2013**, *135*, 3748−3751.
(44) Zhu, Z.; Wu, C.; Liu, H.; Zou, Y.; Zhang, X.; Kang, H.; Yang, C. J.; Tan, W. An Aptamer Cross-Linked Hydrogel as a Colorimetric Platform for Visual Detection. *Angew. Chem., Int. Ed.* **2010**, *49*, 1052−1056.
(45) Dave, N.; Chan, M. Y.; Huang, P.-J. J.; Smith, B. D.; Liu, J. Regenerable DNA-Functionalized Hydrogels for Ultrasensitive, Instrument-Free Mercury(Ii) Detection and Removal in Water. *J. Am. Chem. Soc.* **2010**, *132*, 12668−12673.
(46) Lin, H.; Zou, Y.; Huang, Y.; Chen, J.; Zhang, W. Y.; Zhuang, Z.; Jenkins, G.; Yang, C. J. Dnazyme Crosslinked Hydrogel: A New Platform for Visual Detection of Metal Ions. *Chem. Commun.* **2011**, *47*, 9312−9314.
(47) Guo, W. W.; Qi, X. J.; Orbach, R.; Lu, C. H.; Freage, L.; Mironi-Harpaz, I.; Seliktar, D.; Yang, H. H.; Willner, I. Reversible Ag +-Crosslinked DNA Hydrogels. *Chem. Commun.* **2014**, *50*, 4065−4068.
(48) Guo, W. W.; Orbach, R.; Mironi-Harpaz, I.; Seliktar, D.; Willner, I. Fluorescent DNA Hydrogels Composed of Nucleic Acid-Stabilized Silver Nanoclusters. *Small* **2013**, *9*, 3748−3752.
(49) Sun, L.; Hu, N.; Peng, J.; Chen, L.; Weng, J. Ultrasensitive Detection of Mitochondrial DNA Mutation by Graphene Oxide/DNA Hydrogel Electrode. *Adv. Funct. Mater.* **2014**, *24*, 6905−6913.
(50) Zhang, L.; Lei, J. P.; Liu, L.; Li, C. F.; Ju, H. X. Self-Assembled DNA Hydrogel as Switchable Material for Aptamer-Based Fluorescent Detection of Protein. *Anal. Chem.* **2013**, *85*, 11077−11082.
(51) Huang, Y.; Ma, Y.; Chen, Y.; Wu, X.; Fang, L.; Zhu, Z.; Yang, C. J. Target-Responsive Dnazyme Cross-Linked Hydrogel for Visual Quantitative Detection of Lead. *Anal. Chem.* **2014**, *86*, 11434−11439.
(52) Song, Y.; Zhang, Y.; Bernard, P. E.; Reuben, J. M.; Ueno, N. T.; Arlinghaus, R. B.; Zu, Y.; Qin, L. Multiplexed Volumetric Bar-Chart Chip for Point-of-Care Diagnostics. *Nat. Commun.* **2012**, *3*, 1283.
(53) Zhu, Z.; Guan, Z.; Jia, S.; Lei, Z.; Lin, S.; Zhang, H.; Ma, Y.; Tian, Z.-Q.; Yang, C. J. Au@Pt Nanoparticle Encapsulated Target-Responsive Hydrogel with Volumetric Bar-Chart Chip Readout for Quantitative Point-of-Care Testing. *Angew. Chem., Int. Ed.* **2014**, *53*, 12503−12507.
(54) Frens, G. Controlled Nucleation for the Regulation of the Particle Size in Monodisperse Gold Suspensions. *Nature* **1973**, *241*, 20−22.

DOI: 10.1021/acsami.5b01120
ACS Appl. Mater. Interfaces 2015, 7, 6982−6990